ADAPTIVE CURRENT CONTROL OF VARIABLE RELUCTANCE FINGER GRIPPER

Kenneth Kin-Chung Chan, Michael Shing-Wai Tam, Norbert C. Cheung
Department of Electrical Engineering, Hong Kong Polytechnic University
Hunghom, Kowloon, Hong Kong SAR, China

Abstract

Variable Reluctance (VR) actuators often suffer heavily from non-linear characteristics. With its non-linear torque output, it is difficult to operate and control as a proportional device.

This paper proposes a new adaptive current control scheme for VR actuators employed in force control applications. VR gripper characteristic is first measured and modelled with a non-linear mathematical model. The proposed method with position and current information feedback, linearized the current loop by varying the current control parameters with adaptive pole-zero cancellation scheme and thus obtain a first order response. The method was tested experimentally on a VR gripper.

Keywords
Finger gripper, variable reluctance, adaptive current control.

1 INTRODUCTION

Variable reluctance (VR) actuators are rugged, reliable inexpensive, simple to construct and possess a relatively high torque efficiently [1]. With no permanent magnet, they can operate at hostile environments. With their applications as actuators for the robotics and high-precision industries, they continue to attract much attention in recent years. A VR actuator has a non-linear torque production characteristics; it is difficult to control and operate as a proportional device. The inductance of the VR actuator itself is highly non-linear and has different operating points. To achieve high precision motion control of the VR actuator, the development of a high performance front-end current driver becomes a challenging problem.

In classical PI current control driver, the motor impedance matching technique cannot produce a flat frequency response with varying load impedance. It is because the conventional PI current driver is matched with a particular impedance value of the VR actuator. In many force control applications (e.g. wire-bonding in the semiconductor industry), the force generated by the actuator cannot exhibit any overshoots. In these cases, a better technique for current control is needed.

In this paper, the inductance and position of the VR load is continuously monitored. The measured load impedance and the position information are used to linearize the electrical & mechanical characteristic of the VR actuator. In this way the system is linearized and optimum control can be applied.

2 CURRENT CONTROL OF VR SYSTEMS

The main difficulty of current controller design is due to the non-linearity of VR systems.

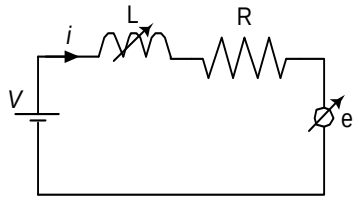

Figure 1. Equivalent VR Gripper magnetic circuit representation

The VR motor can be represented as a resistive and a variable inductive structure. Its voltage equation can be expressed as:

$$\begin{aligned} V &= Ri + \frac{d\lambda(\theta,i)}{dt} \\ &= Ri + \frac{d\lambda(\theta,i)}{di}\cdot\frac{di}{dt} + \frac{d\lambda(\theta,i)}{d\theta}\cdot\frac{d\theta}{dt} \\ &= Ri + L(\theta,i)\cdot\frac{di}{dt} + e(\theta,i,\omega) \end{aligned} \quad (1)$$

where

V	terminal voltage;
R	coil resistance;
i	current;
θ	rotor angle;
λ	flux linkage;
L	inductance;
e	back emf.

For low speed operation, back emf can be omitted and equation (1) can be rewritten as:

$$V = Ri + L(\theta, i) \cdot \frac{di}{dt} \qquad (2)$$

Equation (1) clearly shows that the motor inductance L is a function of θ and i. Designing an optimum current controller with a varying inductive load becomes a challenging problem. With a varying load L, the di/dt term, which is a dominant term in the motor's dynamic current response, also varies. Figure below shows a typical inductance profile for a VR motor.

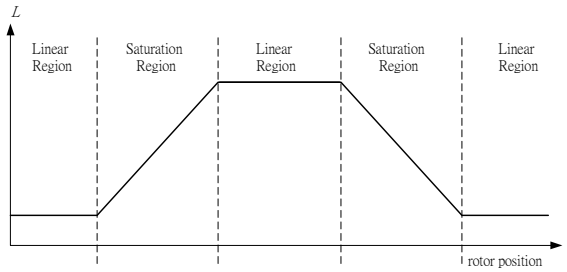

Figure 2. A typical inductance profile for VR motor.

Typically, two types of current control schemes are commonly used. They are hystersis control, as shown in figure 3(a) and PID control, as shown in figure 3(b) [2, 3]. Hystersis control is easy to implement and robust to load variations [2]. However, it suffers from large current ripple, especially at low current levels. PID control has less current ripple [3]. It provides a better solution for converter design and noise prediction, but it fails to adapt to load variations, especially during fast current dynamics.

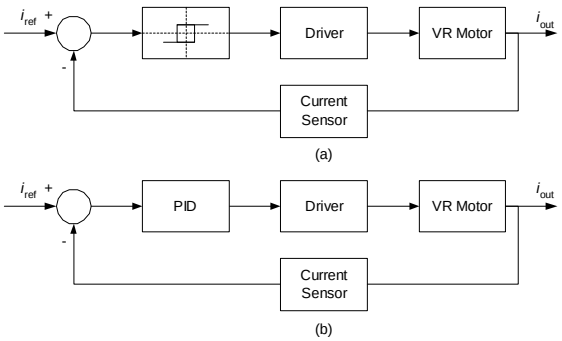

Figure 3. Current Control Block Diagram for VR motors (a) Hystersis Control; (b) PID Control.

3 ADAPTIVE CURRENT CONTROL

The block diagram for proposed adaptive current control scheme is shown in figure 4. The main objective is to linearize the motor's non-linear characteristics with adaptive pole-zero cancellation method.

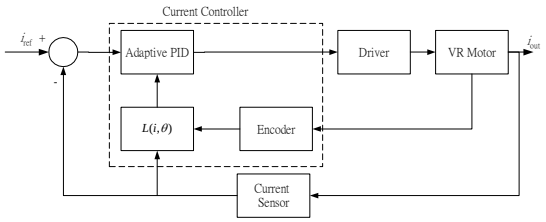

Figure 4. Adaptive Current Control Block Diagram for VR motors

The proposed current controller structure is similar to classical PI control structure. Instead of having a simple PID control, an adaptive current controller as shown in figure 4 replaces it.

Motor flux linkage relationship against current and rotor position is first measured. Its inductance profile is then modelled with a non-linear function, $L(\theta, i)$. Thus, load variation can be calculated on-line with encoder and current feedback. Therefore, PI parameters can be varied and adept to load variation.

4 VR FINGER GRIPPER

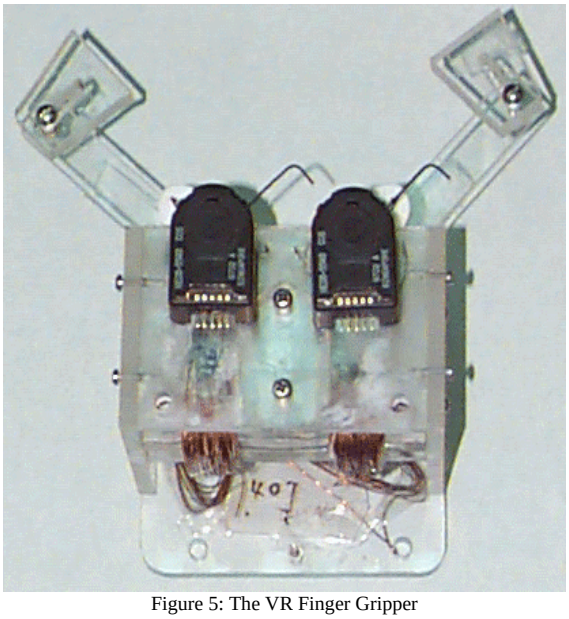

Figure 5: The VR Finger Gripper

Figure 5 shows the VR actuator used in the project. It consists of two rotary elements, each attached to a finger. The actuator contains two coils with 400 turn windings each.

The moving rotors are mounted onto two individual shafts, whose axes are normal to the plane of the diagram, so that it may rotate freely between the poles of the stator. Both the rotors and stators are made up of laminated mild steel to reduce eddy current effects.

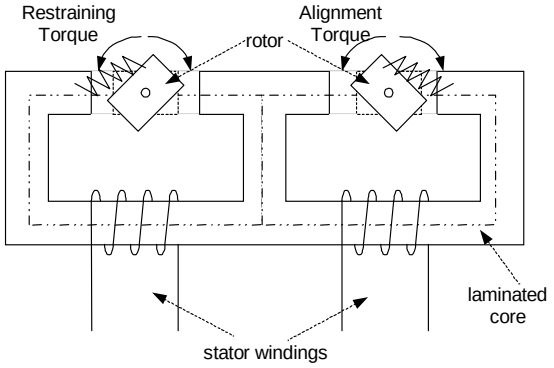

Figure 6: Top View of Rotary VR Gripper

Two fingers of the gripper, shown in Figure 6, are 90mm long and spring loaded, which allows bi-directional movement from the single direction excitation of the coils. When currents are applied to the stator windings, the rotors rotate away from initial positions to reduce their reluctance by alignment torque. The rotors eventually stay still when alignment torque comes into equilibrium with restraining torque provided by the spring. When the fingers rotate by 70°, the fingertips would be closed and the rotors are in fully aligned positions. Incremental rotary encoders are mounted on the shafts to measure rotor positions with a resolution of 0.09°.

5 MODELLING

The VR gripper inductance can be represented by the following exponential Equation [3].

$$\begin{aligned} L(\theta,i) &= \frac{d\lambda(\theta,i)}{di} \\ &= \frac{d\lambda_s(1-e^{-f(\theta)i})}{di} \\ &= f(\theta)e^{-f(\theta)i} \end{aligned} \tag{3}$$

where $f(\theta) = a + b\cos\theta + c\cos 2\theta + d\sin\theta + e\sin 2\theta$ and λ_s is unity [6].

Figure 7 shows the relationship between the inductance of the VR gripper with rotor angles. Due to the large air gap presented in the system, L is insensitive to change current levels. Therefore, $L(\theta,i)$ can be simplified to $L(\theta)$ and modelled with a third order polynomial curve fitting least square error method.

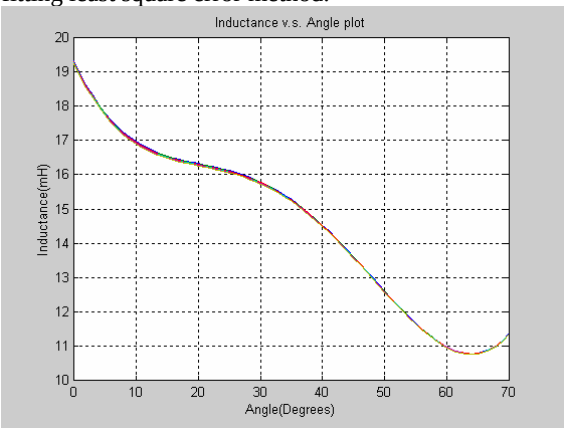

Figure 7: VR Gripper Inductance Profile vs. Rotor Angle

By taking Laplace Transform of Equation (2),

$$\begin{aligned} \frac{I(s)}{V(s)} &= \frac{1}{sL(\theta)+R} \\ G(s) &= \frac{\frac{1}{L(\theta)}}{s+\frac{R}{L(\theta)}} \end{aligned} \tag{4}$$

The transfer function, *T(s)*, of the PI controller is:

$$\begin{aligned} T(s) &= K_p + \frac{K_i}{s} \\ &= \frac{K_p}{s}(s + \frac{K_i}{K_p}) \end{aligned} \tag{5}$$

The forward transfer function, C(s), can therefore be written as:

$$\begin{aligned} C(s) &= T(s)\,G(s) \\ &= \left(\frac{K_p}{s}(s + \frac{K_i}{K_p})\right)\left(\frac{\frac{1}{L(\theta)}}{s+\frac{R}{L(\theta)}}\right) \\ &= \left(\frac{K_p}{L(\theta)s}\right)\left(\frac{(s + \frac{K_i}{K_p})}{(s+\frac{R}{L(\theta)})}\right) \end{aligned} \tag{6}$$

By matching $\frac{K_i}{K_p} = \frac{R}{L(\theta)}$, the pole and zero of Equation (6) can be cancelled out and the closed-current-loop transfer function $I_c(s)$ can be reduced to a first order one as:

$$I_c(s) = \frac{\frac{K_p}{L(\theta)}}{s + \frac{K_p}{L(\theta)}} \quad (7)$$

If ω_n is the required bandwidth of the current loop, the K_p & K_i can be found as:

$$K_p = \omega_n L(\theta) \quad (8)$$

&

$$K_i = \omega_n R \quad (9)$$

While R is the resistance of the VR actuator and is a constant. It is therefore an adaptive PI current controller can be implemented with the K_p control parameter continuously modified by the feedback information $L(\theta)$. The resulting adaptive PI current control loop will have a consistence current response that is independent to the change of the reluctance of the actuator. The position of the VR actuator is monitored by a position sensor that in turn gives inductance information through the $L(\theta)$ function that obtained experimentally.

6 SIMULATION

The comparison between the performance of the adaptive current control and the PI current control is done by using the MatLab "simulink". The block diagram of the simulink model is shown in Figure 8. The PI current loop is tuned to a medium load inductance value and has same bandwidth as the adaptive PI loop. As can been seen in Figure 9, the adaptive loop always has a better response than the PI in terms of symmetry and overshoot.

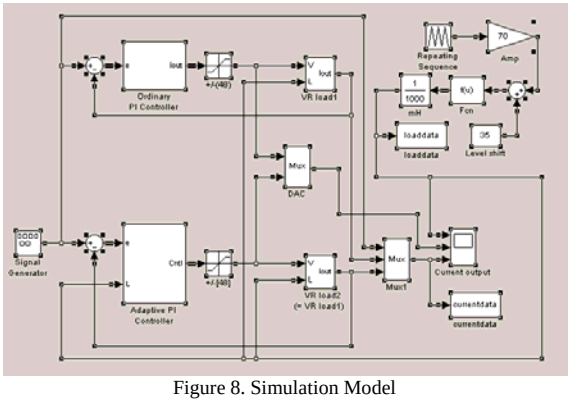

Figure 8. Simulation Model

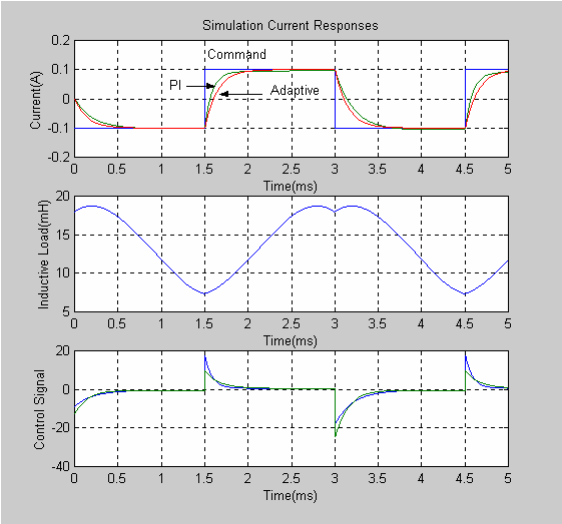

Figure 9. Simulated Responses

7 IMPLEMENTATION

7.1 Controller

A dSPACE DS1102 card is used as the current controller, which has an on-board TMS320C31 DSP with 60 MHz for real-time computation. This controller card package also comes with the data-monitoring and software control tools. In connecting with MATLAB real-time workshop and SIMULINK, a PC-based fast control prototype can be produced.

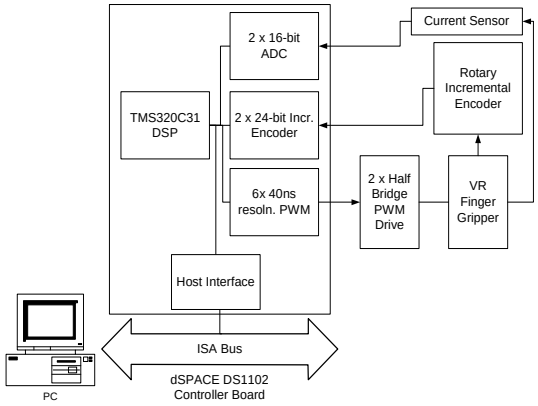

Figure 10: Experimental Set Up

With 16-bits analogue and 24-bits encoder input channels, stator currents and system positions can be fed back to the controller. The controller can read in these inputs at each sampling interval, calculate the control signal by the controller and issue at its PWM output channels.

7.2 Switching Power Stage

The switching power stage converts controlled PWM signals into the PWM high voltage source and excites the stator coils. The conditioned current signal and encoder position is sampled by the controller for the calculation of the next controlled signal. Figure 11 below shows the switching power stage used in this project.

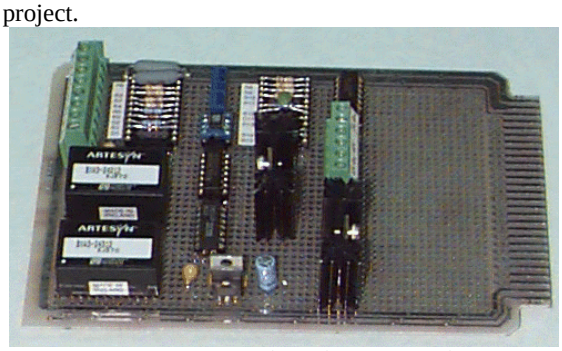

Figure 11. Diagram of a Half Bridge Amplifier

The PWM driver used in this project is a pair of high-low side power MOSFET, IRF740, half-bridge amplifier. It acts as a current amplifier for the motor. It has fewer components than full bridge amplifier and has a true ground that makes current measurement much simpler. The current feedback circuit has a gain of 1.2A/V. The motor side & logic side is electrically isolated by the opto-couplers that may introduce about 300nS delay. Dead-time delay protection against cross conduction of the high-low side MOSFETS is introduced.

7.3 Results

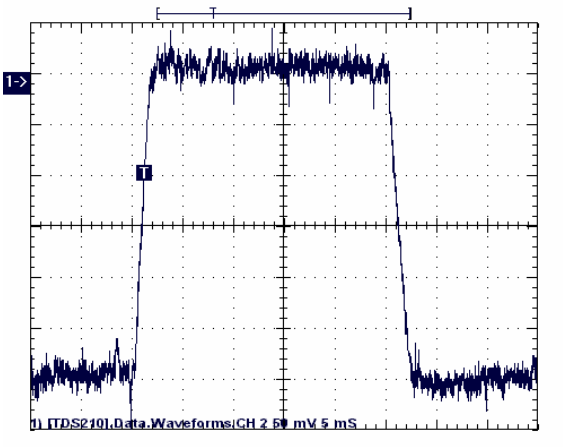

Figure 12. Responses with high inductance (both method)

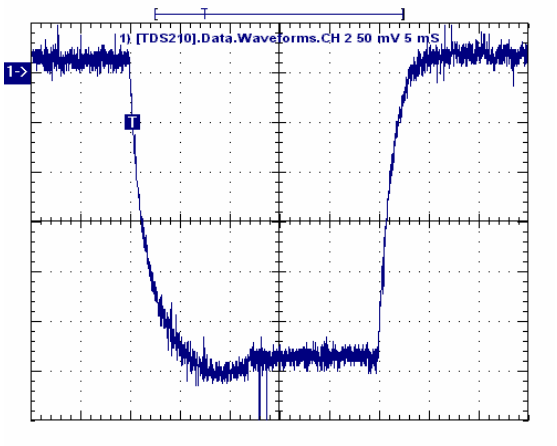

Figure 13. PI current response with 50% inductance drop

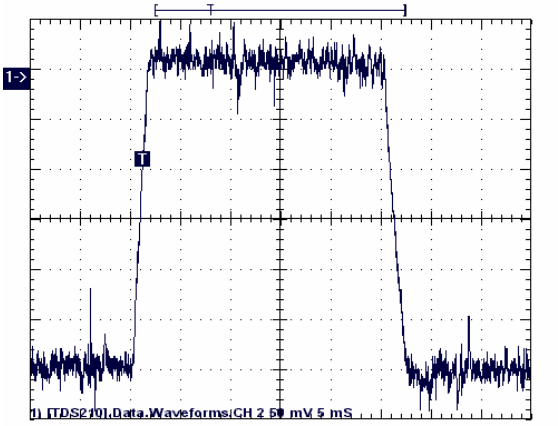

Figure 14. Adaptive PI current response with 50% inductance drop

Figure 12 is the current response of the PI and adaptive PI current loop. It shows a good current tracking as both systems are matched with that particular high inductance value. The current response of the PI and adaptive PI loop with 50% drop of the inductance value is shown in Figure 13 and Figure 14 respectively. The adaptive PI loop exhibits a consistence response while the PI loop has a slight overshoot.

8 CONCLUSION

This paper describes the development of the adaptive current control loop for current drive of the variable reluctance finger gripper. The fully digital PI current control loop and the adaptive PI current control loop has been implemented, tested and verified. Both current loops provide satisfactory results for up 30% of inductance change. As the change goes up to 50%, there is a deficiency of the PI loop in tracking the

current command profile, while the adaptive current loop shows a consistence response over a 50% inductance variation. Therefore the adaptive PI current controller has been successfully developed and it can provide superior performance on a load with wide variation in inductance. This is especially useful in the current control of switched reluctance motors, because their reluctance change can be as high as 3-5 times.

REFERENCES

[1] T.J.E. Miller. *Switched reluctance motor and their control*. Magne Physics Publishing and Clarendon Press, Oxford, 1993.

[2] G.R. Slemon and A. Staughen. *Electric Machines.* Addison Wesley, 1982.

[3] K. Russa, I. Husain and M. Elbuluk. Torque Ripple Minization in Switched Reluctance Machines Over a Wide Speed Range. *IEEE Industry Applications Society Annual Meeting*, Oct., 1997. P668-675.

[4] G. Gallegos-López, P. C. Kjaer and T. J. E. Miller. High-Grade Position Estimation for SRM Drives Using Flux Linkage/Current Correction Model. *IEEE Trans. on Indust. App*., Vol.35, No. 4, p859-869, Jul-Aug. 1999.

[5] G. F. Franklin, J. D. Powell and A. Emami-Naeini. *Feedback Control of Dynamic Systems*. Addison Wesley, 1991.

[6] S. Mir, I. Husain and M. E. Elbuluk. Switched Reluctance Motor Modelling with On-Line Parameter Identification IEEE Trans. on Ind. App., Vol. 34, No. 4, pp776-783, Jul./Aug. 1998.